ANALYTICAL SCIENCES DECEMBER 2017, VOL. 33

Original Papers

Layer Caused an Anisotropic Terahertz Response of a 3D-printed Simulative Shale Core

Xinyang MIAO,*, Limei GUAN,** Rima BAO,*,**† Yizhang LI,** Honglei ZHAN,** Kun ZHAO,*,** Xiaodong WANG,*** and Fan XU*****

**State Key Laboratory of Petroleum Resources and Prospecting, China University of Petroleum, Beijing 102249, China*
***Beijing Key Laboratory of Optical Detection Technology for Oil and Gas, China University of Petroleum, Beijing 102249, China*
****School of Physics and Optoelectronic Engineering, Yangtze University, Jingzhou 434023, China*

Energy demands have motivated the development of shale formations as significant unconventional reservoirs. The anisotropy of shales plays a significant role in both the mechanical behavior and engineering activities. Alternating layers presented in shales affect the propagation of waves, causing anisotropy at various frequencies. Simplifying the complicated interior structures of shales is conducive to characterize the anisotropic properties. Therefore, simulative shale core samples were designed and fabricated using additive manufacturing processes, and layer-caused dielectric anisotropy was investigated by terahertz (THz) time-domain spectroscopy. On the basis of effective medium theory, the change of the optical length caused by refraction of rays was discussed and modeled. It is believed that the refraction of rays at the interfaces is the source of THz propagation anisotropy in the multilayered structure, and the anisotropy degree is mainly influenced by the layer thickness as well as the refractive index.

Keywords Anisotropy, shale, terahertz, additive manufacturing

(Received May 3, 2017; Accepted August 14, 2017; Published December 10, 2017)

Introduction

Shales, acting as cap rocks of conventional reservoirs formations, have been found in most global sedimentary basins. Most recently, energy demands have motivated the development of shale formations as significant unconventional reservoirs. Layers, one of the most common structural features of sedimentary rocks, have been the focus of numerous studies by both geologists and engineers.[1] As the most common of sedimentary rocks, shales have been estimated to form ~75% of all sedimentary rocks on earth.[2] They are fine-grained sedimentary rocks composed primarily of clay, organics, as well as hard minerals such as quartz, feldspar, and pyrite.[3] Owing to various combined effects of partial alignment of platy clay particles, layering, micro-cracks, low-aspect-ratio pores, and kerogen inclusions, shales are often highly anisotropic.[4] The anisotropy of shales plays a significant role in both the mechanical behavior and engineering activities. For hydraulic fracturing, the noted anisotropy affects drilling, borehole stability as well as perforation orientation, and also controls the initiation and propagation of hydraulic fractures, and further impacts on the flow and leakage of the fracturing fluid.[5] Thus, the influences in the anisotropy of shales must be taken into account for traditional and advanced geophysical exploration technologies. Ultrasonic systems have been widely used to study shale anisotropy in the laboratory.[6,7] These studies have mainly focused on the elastic properties of shales, and have revealed that the preferential alignment of clay minerals and cracks is the major factor leading to the intrinsic anisotropy of shales. Organics' shapes and distribution exhibit some elongation parallel with bedding direction, making the organics in shales an important source of elastic anisotropy.[8] Besides, the scanning electron microscopy (SEM) technique has been commonly used for the microstructure determination of shales.[9] The planes perpendicular and parallel to the bedding were analyzed by SEM, showing some patchy kaolinite and acicular illite with preferred orientations parallel to the bedding. An oblique-incidence reflectivity difference (OIRD) technique was utilized to characterize the layered distribution of the dielectric properties in shales, indicating that directional changes of the dielectric and surface properties resulted due to micro-cracks and particle orientation.[10] The presence of alternating layers in shales also affects the propagation of waves, causing anisotropy at various frequencies.[11] Shales have complex layer structures consisting of various mineral components and kerogen contents, and simplifying the complicated interior structure of shale is conducive to characterizing the anisotropic properties.[12] In recent years, additive manufacturing (AM) technology has become a powerful tool for direct digital manufacturing.[13] Being well known as "3D printing", the technique possesses the advantages of accuracy and cost-efficiency. Based on the data from three-dimensional models, the materials can be rapidly

† To whom correspondence should be addressed.
E-mail: brm22@163.com

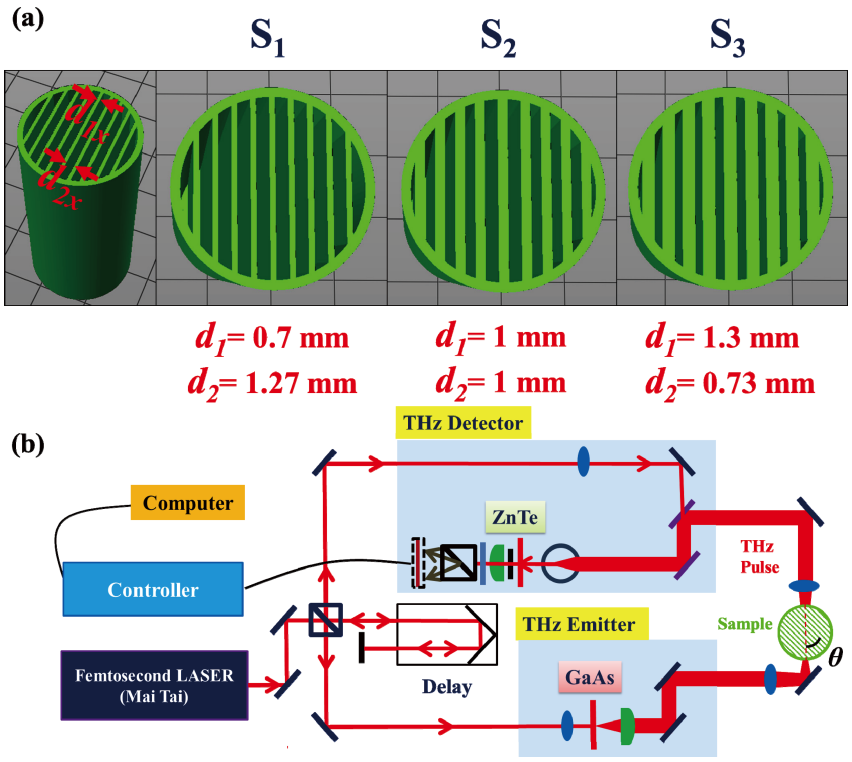

Fig. 1 (a) 3D models of the simulated "shale core". (b) Top-view, schematic of the experimental setup, in which θ is defined as the angle between the input orientation of terahertz ray and the layer.

solidified to fabricate physical objects. AM also provides an innovative approach to study rock.[14] This technique has been used to fabricate test specimens of complicated rock structures with cracks and joints to investigate the stress changes in the process of mining, showing a promising way to quantify and visualize the complex fracture structures and their influences on the stress distribution of underground rocks.[15]

Since the layering in shales was on the sub-millimeter scale, terahertz (THz) wave, with wavelengths of 30 μm – 3 mm and frequencies of 0.1 – 10 THz, it is a sensitive tool for studying the effect of alternating layers on the degree of anisotropy. Owing to the unique advantages, this technique is expected to be a "silver bullet" in various aspects of oil and gas resources,[16] especially in reservoirs and rocks.[17] At present, THz-TDS has been applied to investigating the optical properties of marble, sandstone, and limestone.[18] The dielectric properties of montmorillonite clay,[19] micaceous clay,[20] kaolinite, halloysite,[21] and clay-based polyamide nanocomposite films were measured at the THz region.[22] Meanwhile, the THz technique has also been employed to study the anisotropic response of materials. Various crystals and alternating structures have been studied to exhibit THz birefringence.[23] In our previous work,[24] anisotropic responses of oil shales were initially studied by THz-time domain spectroscopy (THz-TDS). The refractive index anisotropies of the oil shales were compared with each other and plotted as a function of the oil yield, showing that the increase of organic matter has promoted anisotropy in the THz range. In this article, we consider the anisotropic response of 3D-printed simulated "shale core" by THz-TDS. The refraction of the ray at the interfaces was considered and modeled to figure out the source of THz propagation anisotropy in the multilayered structure.

Experimental

Actual shales are characterized by breaks along thin laminaes or parallel layering less than 1 cm in thickness, with layers composed of different minerals or liquids.[2,5] Here, in this research, we designed cylindrical structures consisting of alternating layers made of solid and air gaps to simulate the shale core. We focused on the anisotropic response caused by the layer in this study, herein, the regular structures of the 3D printed samples were beneficial to the theoretical analysis and helpful to exclude other factors. Simulative samples were designed and fabricated using the AM processes started from a software model illustrated in Fig. 1(a). Three cylindrical structures (numbered S_1, S_2 and S_3) consisting of alternating layers made of solid and air gaps were designed with the diameter 21 mm and the wall thickness 1 mm. The number of the layers in them were uniform but the thicknesses varied. 3D printing of the models was achieved by a XYZ Printing™ 3D printer (da Vinci 2.0) based on a technique of curing polymer named fused deposition modeling technology (FDM). Acrylonitrile-butadiene-styrene (ABS), which is a kind of thermoplastic material commonly employed in FDM, was used as the raw material of the samples. The material was firstly heated and melted, then extruded and solidified quickly.

We used a THz-TDS setup with the frequency range 0.1 – 3 THz based on photoconductive antenna and electro-optical sampling to study the layer-caused dielectric anisotropy. Figure 1(b) appears in a schematic drawing of the experimental setup. An femtosecond laser beam (800 nm) was split into two beams, the pump beam was focused onto the surface of a biased GaAs photo-conductive antenna for THz generation and the probe beam for electro-optic detection. THz pulses were

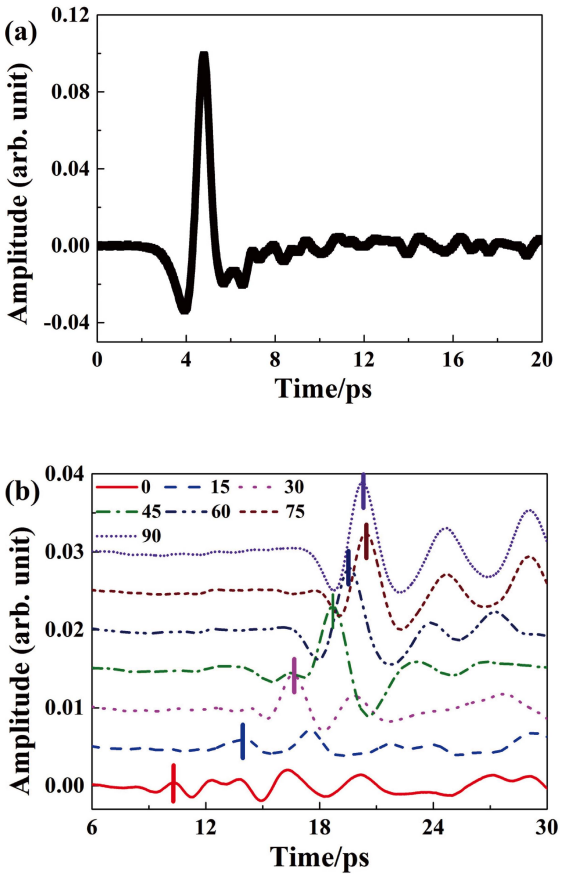

Fig. 2 Time-domain spectra of the (a) reference and (b) S_1 with varies angles from 0 to 90°. The short vertical bar marks the first THz waveform signal for each angle.

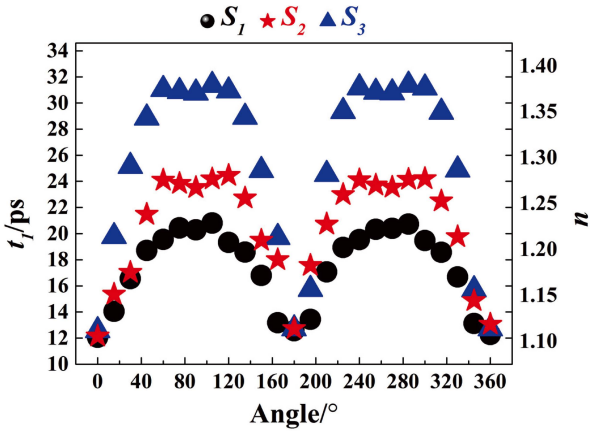

Fig. 3 t_1 and n change as a function of the rotation angle.

focused onto a sample by an optical lens, and met the probe laser beam at the ZnTe crystal in the THz detector. The 3D-printed model was installed in the center of a manually rotational stage, and the emitter and detector beams were aligned on the antipodes for a transmission experiment. The experiments were performed under air atmosphere at a temperature of 294.1 K and a humidity of ~10% with a signal-to-noise ratio of ~1000 during the measurement. The setup provides a direct measurement of THz wave propagation along the diameter of the circle, and hence the angle dependent THz parameters can be obtained. The rotation angles (θ) were defined as the angles between the input orientation of THz ray and the layer. THz-TDS of the air was initially measured as the reference signal, and the samples with different d_1 and d_2 were rotated and tested one by one.

Results and Discussion

As an example of the raw THz data, time-domain spectra of S_1 with varies θ from 0 to 90° are presented in Fig. 2. Waveforms of the sample with different θ are variant from each other. The observed THz wave signals correspond to direct waves with different optical distances owing to the circular structure followed by the scattered waves arriving at later times. The delay time (t_1) of the first peak is located (marked by the short vertical line in the figure) and extracted. It is obvious that the time delay of the THz wave is strongly dependent upon θ for the arrival of the first THz signal. t_1 gradually increases with rotation from 0 to 90°. To be specific, t_1 of S_1 at the first signal is 12.06, 14.05, 16.55, 18.72, 19.56, 20.43 and 20.28 ps with θ equals 0, 15, 30, 45, 60, 75 and 90° in the figure, respectively. The same measurements have also been performed for S_2 and S_3; the group angle dependent t_1 are presented in Fig. 3. We then calculated the effective refractive index (n) by t_1 as well as the reference (t_0),

$$n = 1 + \frac{c \times (t_1 - t_0)}{D_0}, \quad (1)$$

in which c is the speed of light, and D_0 is the external diameter of the circle. According to Eq. (1), n is related to t_1; thus the variation trends of n are consistent with t_1, as shown in Fig. 3. It is clear from the figure that all the samples have significant t_1 and n anisotropy, meanwhile, there is a data symmetry every 180° owing to the geometry of the layer consisted samples. In an angular period of 180°, both t_1 and n basically increase in the first half from 0 to 60°, and the fall is symmetric from 120 to 180°. At angles of 60 - 120°, the values are basically invariant, especially for S_2 and S_3. Besides, both of them are approximately the same for all three samples with the transmission direction parallel to the layer (at 0, 180 and 360°). The average values of t_1 are 12.29, 12.64 and 12.66 ps, as well as n 1.10, 1.11 and 1.11, respectively. However, different variation curves can be observed among the samples. The maximum t_1 and n raised with increasing d_1.

In order to verify the experimental result, we conduct an analysis of the THz ray propagation. Given that the ray is subject to lateral movement after going through the solid part, the directions of rays intro or inter the layers are consistent respectively. Thus we propose an imaginary solid layer and an air layer to simulate the layered 3D-printed models, whose thicknesses are the sum of solid and air layers that THz ray penetrates, as shown in Fig. 4. In this equivalent model, the original optical length separated in same sort of layers are aligned without any change in the total optical length or incident angle. A rectangle, whose diagonal is the diameter of the circumscribed circular intercept, is depicted to subsume the trace of the ray within the sample. The ray enters this rectangle along its diagonal at first, and then it refracts when traveling through the interface due to different n values on both sides of the interface. We managed to figure out the optical length in two equivalent layers, and then applied effective medium

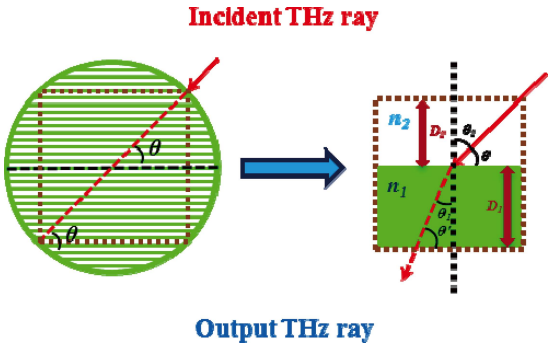

Fig. 4 Schematic diagram of the model based on the effective medium theory, in which n_1 and n_2 as well as D_1 and D_2 represent the refractive index as well as the effective thickness of the solid layers and air layers, respectively.

theories to calculate n. As we suppose, the calculated n should be close to the measured one.

We define a reference plane which is parallel to any layer and the entire sample is symmetry with respect to this plane. It is evident that two surfaces of both the air layer and the solid layer are parallel to the reference plane. The distance between two surfaces of a solid layer is the effective thickness for discrete solid layers which is defined as D_1. Similarly, the effective thickness for discrete air layers is marked as D_2 (as shown in Fig. 4). On account of the angle between the incident ray and the reference plane (defined as θ), as well as the angle between the refracted ray and the reference plane (defined as θ'), the actual length of the ray within the solid layer (L_1) and air layer (L_2) ought to be

$$L_1 = \frac{D_1}{|\sin\theta'|} \tag{2}$$

and

$$L_2 = \frac{D_2}{|\sin\theta|}, \tag{3}$$

respectively. According to the refractive index of the ABS material and the air (defined as n_1 and n_2), a relationship was built based on the equivalent optical length

$$n_1L_1 + n_2L_2 + 2n_1D' = n(L_1 + L_2 + 2D'), \tag{4}$$

where D' is the thickness of the wall. On the basis of the Snell's law as well as the refracting angle θ_1 and the incident angle θ_2, we obtained

$$n_1\sin\theta_1 = n_2\sin\theta_2. \tag{5}$$

Then, according to the relationship between the angles shown in Fig. 4,

$$\sin\theta' = \sqrt{1-\left(\frac{n_2}{n_1}\right)^2\cos^2\theta}, \tag{6}$$

by applying Eqs. (2), (3) and (6) to Eq. (4), we obtained

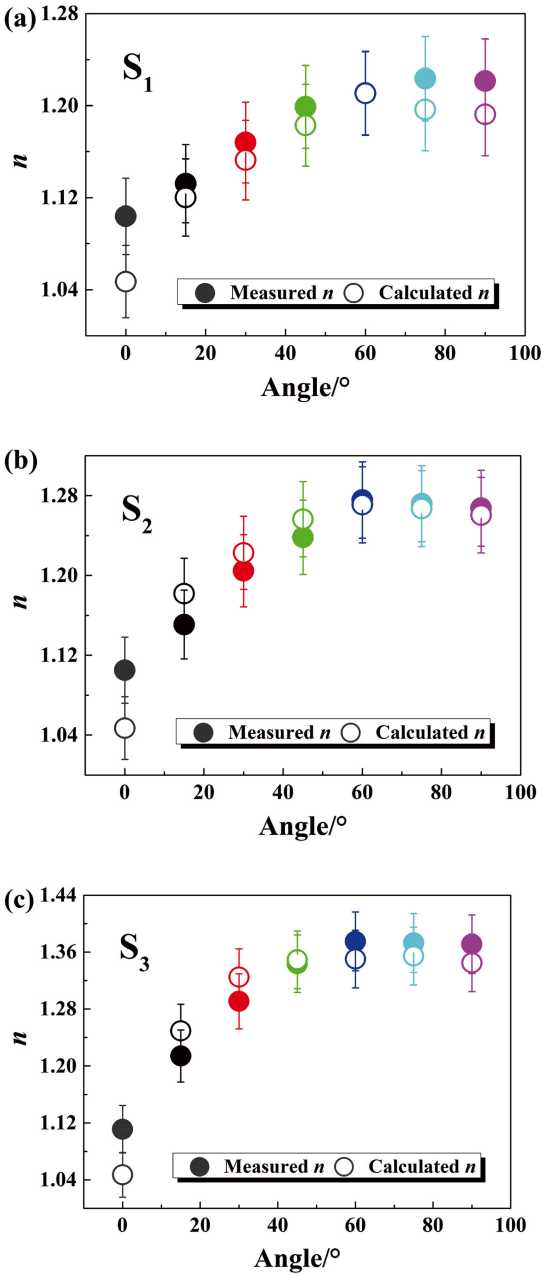

Fig. 5 Measured n and calculated n as a function of the angle for (a) S_1, (b) S_2 and (c) S_3, respectively. The solid and hollow circles represent the experiment and simulation results, respectively. Error bars represent 3% of the data values.

$$n = \frac{\dfrac{n_2D_2}{|\sin\theta|} + \dfrac{n_1D_1}{\sqrt{1-\left(\dfrac{n_2}{n_1}\right)^2\cos^2\theta}} + 2n_1D'}{\left(\dfrac{D_2}{|\sin\theta|} + \dfrac{D_1}{\sqrt{1-\left(\dfrac{n_2}{n_1}\right)^2\cos^2\theta}}\right)}. \tag{7}$$

The theoretical results of n at varies angles of 15, 30, 45, 60, 75 and 90° were calculated by Eq. (7) with the THz-TDS measured refractive index of air ($n_2 = 1$) and ABS material ($n_1 = \sim 1.56$) used in this experiment. As plotted in Fig. 5, the calculated values show a good agreement with that of the experiment. The maximum relative errors between the calculated and

experimental results are no larger than 3%. Besides, in the cases of $\theta = 0^\circ$, part of the rays penetrate air layers and approach the detector at first, followed by those travelling through solid layers; n is approximately calculated by the length of air layer and the thickness of the wall. Actually, owing to a slight deflection of the rays, the measured n is larger than the calculated one under this circumstance.

It is obvious that the presence of alternating layers in the model has a strong influence on the degree of dielectric anisotropy. The results have also shown an attenuation of n in the THz propagation direction parallel to the layering compared with that perpendicular to the layering. According to an analysis of THz ray propagation as well as experimental data, we consider that the change of optical length, which results refraction of the ray at the interfaces, led to the n anisotropy of the models. As described in Eqs. (2) and (6), the deflection of THz ray shortens the actual optical length within the solid layers, and such deflection diminishes with the increase of θ in the range of 0 – 90°, while the proportion of the optical length within the solid raises. Since n_1 is larger than n_2, n augments gradually with the increase of θ from 0 to 90°.

With a lack of thorough understanding of anisotropy theoretically, the anisotropic properties of shales have been of long-standing interest, and the sources of elastic anisotropy are inherently complex and difficult to discriminate.[5] Ultrasonic measurements under variable saturation and pressure conditions in the laboratory have revealed that anisotropy of elastic wave propagation is caused mainly by the preferential alignment of mineral grains and thin layers.[6,7] Near cracks, the effective density and thickness are clearly different from those at other locations. Such heterogeneity is minimized at high confining pressures upon the closure of cracks.[8,10] Moreover, solid organic matter is also a strong source of anisotropy in shales owing to the elongation distribution of organic matter parallel with the bedding.[2,5] The organic matter appears to have little intrinsic birefringence; however, organic matter, such as kerogen, has always exhibited some elongation parallel with the bedding, which is caused by lithostatic overburden and deformation, and by the original orientation when kerogen first deposits.[8] For electromagnetic waves, the presence of alternating layers in shales has a strong influence on the degree of dielectric anisotropy.[11] In our previous study, we modeled the oil shale samples as a uniaxial birefringent medium, and discussed the organic matter-dependent n anisotropy.[23] Here in this work, the effect of the layer structure is investigated. The refraction of the ray at the interfaces is believed to be the source of anisotropy, which was never considered in previous studies. In this circumstance, the anisotropy degree is mainly influenced by the layer thickness and the refractive index. In addition, for shales consisting of kerogen-rich and kerogen-poor layers, the refractive index of the layers is mainly decided based on the organic matter content. For a better guidance of the development of shale, the relationship between the anisotropy caused by refraction and the organic matter content should be investigated in the future to quantify the anisotropic properties of shales.

Conclusions

In conclusion, THz-TDS was employed to investigate the anisotropic response of 3D-printed multilayered samples. On the basis of the effective medium theory, the change of the optical length caused by refraction of the ray was considered and modeled. It is believed that the refraction of the ray at the interfaces is the source of THz propagation anisotropy in the multilayered structure, and the anisotropy degree is mainly influenced by the layer thickness and the refractive index. The results prove that THz-TDS combined with the AM technique is willing to be an effective means for researching the anisotropy of shales.

Acknowledgements

This work was supported by the National Nature Science Foundation of China (Grant Nos. 61405259 and 11574401), the Science Foundation of China University of Petroleum, Beijing (No. 2462017YJRC029).

References

1. P. Wild and S. Crampin, *Geophys. J. Int.*, **1991**, *107*, 513.
2. C. M. Sayers, *J. Geophys. Res.*, **1994**, *99*, 767.
3. S. Han, J. Zhang, Y. Li, B. Horsfield, X. Tang, W. Jiang, and Q. Chen, *Energ. Fuels*, **2013**, *27*, 2933.
4. A. Zhubayev, M. E. Houben, D. M. J. Smeulders, and A. Barnhoorn, *Geophysics*, **2016**, *81*, D45.
5. L. Vernik and X. Liu, *Geophysics*, **1997**, *62*, 521.
6. T. E. Blum, L. Adam, and K. V. Wijk, *Geophysics*, **2013**, *78*, C25.
7. C. D. Piane, D. N. Dewhurst, A. F. Siggins, and M. D. Raven, *Geophys. J. Int.*, **2011**, *184*, 897.
8. A. M. Allan, W. Kanitpanyacharoen, and T. Vanorio, *Geophysics*, **2015**, *80*, C73.
9. B. T. Lin and A. B. Cerato, *Eng. Geol.*, **2014**, *177*, 66.
10. H. L. Zhan, J. Wang, K. Zhao, H. B. Lu, K. J. Jin, L. He, G. Z. Yang, and L. Z. Xiao, *Sci. Rep.*, **2016**, *6*, 39306.
11. J. A. Scales and M. Batzle, *Appl. Phys. Lett.*, **2006**, *89*, 024102.
12. W. Liu, D. Wang, and Q. Su, *Nat. Gas Geosci.*, **2016**, *27*, 1374.
13. B. C. Gross, J. L. Erkal, S. Y. Lockwood, C. Chen, and D. M. Spence, *Anal. Chem.*, **2014**, *86*, 3240.
14. J. Chao and G. F. Zhao, *Rock Mec. Rock Eng.*, **2015**, *48*, 1041.
15. K. C. Bennett, L. A. Berla, W. D. Nix, and R. I. Borja, *Acta Geotech.*, **2015**, *10*, 1.
16. X. Y. Miao, H. L. Zhan, and K. Zhao, *Sci. China Phys. Mech. Astron.*, **2017**, *60*, 024231.
17. R. M. Bao, Z. K. Wu, F. Wang, X. Y. Miao, and C. J. Feng, *Anal. Sci.*, **2017**, *33*, 95.
18. M. Schwerdtfeger, E. Castro-Camus, K. Krugener, W. Viol, and M. Koch, *Appl. Optics.*, **2013**, *52*, 375.
19. I. Wilke, V. Ramanathan, J. LaChance, A. Tamalonis, M. Aldersley, and P. C. Joshi, *Appl. Clay Sci.*, **2014**, *87*, 61.
20. M. Janek, M. Matejdes, V. Szöcs, I. Bugar, A. Gaál, D. Velič, and J. Darmo, *Philos. Mag.*, **2010**, *90*, 2399.
21. D. Zich, T. Zacher, J. Darmo, V. Szöcs, D. Lorenc, and M. Janek, *Vib. Spectrosc.*, **2013**, *69*, 1.
22. N. Nagai, T. Imai, R. Fukasawa, K. Kato, and K. Yamaguchi, *Appl. Phys. Lett.*, **2004**, *85*, 4010.
23. T. Arikawa, Q. Zhang, L. Ren, A. A. Belyanin, and J. Konoet, *J. Infrared Millim. Te.*, **2013**, *34*, 724.
24. X. Y. Miao, H. L. Zhan, K. Zhao, Y. Z. Li, Q. Sun and R. M. Bao, *Energ. Fuels*, **2016**, *30*, 10365.